

## Supporting Information

### **Targeted Deflecting Zn<sup>2+</sup> Migration Trajectory by Piezomagnetic Effect to Enable Horizontal Zn Deposition**

Chenming Zhou,<sup>ac</sup> Zhezhong Zhang,<sup>ac</sup> Mu Zhang,<sup>ac</sup> Xudong Sun,<sup>\*ac</sup> Jun Zhang,<sup>ac</sup> Gang Huang<sup>\*b</sup> and  
Zhaolin Na<sup>\*ac</sup>

<sup>a</sup>Key Laboratory for Anisotropy and Texture of Materials, School of Materials Science and Engineering, Northeastern University, Shenyang 110819, P. R. China.

<sup>b</sup>State Key Laboratory of Rare Earth Resource Utilization, Changchun Institute of Applied Chemistry, Chinese Academy of Sciences, Changchun, 130022, P. R. China.

<sup>c</sup>Foshan Graduate School of Innovation, Northeastern University, Foshan, 528311, P. R. China.

## Experimental Section

**Preparation of nanoparticles:** The formation of  $\text{CoFe}_2\text{O}_4$  magnetic nanoparticles were based on a hydrothermal method. Typically, 0.005 mol  $\text{Co}(\text{NO}_3)_2 \cdot 6\text{H}_2\text{O}$  (98.5%, Sigma-Aldrich), and 0.01 mol  $\text{Fe}(\text{NO}_3)_3 \cdot 9\text{H}_2\text{O}$  (98.5%, Sigma-Aldrich) were added into the 60 mL deionized water to form a mixed solution and stirred at 300 rpm for 60 min. Then, amount of NaOH (98%, Sigma-Aldrich) was rapidly added into the mixed solution and adjusted the solution pH to 12, stirring with a mechanical stirrer at stirring speed of 300 rpm for another 60 min at 70 °C. And then, the dark brown solution was transferred into a 100 mL of Teflon-lined stainless-steel autoclave, maintaining at temperature of 160 °C for 12 h.

**Preparation of CFO artificial protective layer on Zn foil:** To obtain CFO-Zn electrode, the synthesized CFO nanoparticles and polyvinylidene fluoride (PVDF, average Mn ~44080) with a weight ratio of 8:2 were mixed thoroughly in a proper amount of 1-methyl-2-pyrrolidone (NMP, 99.5%, Alfa Aesar). Afterward, the as-prepared slurry was uniformly coated onto Zn foil (100 or 20  $\mu\text{m}$ ) by doctor blading method, which was transferred into a vacuum oven (70 °C, 12 h) to perfectly remove the NMP solvent prior to use.

**Preparation of  $\text{V}_2\text{O}_5\text{-NH}_4^+$  nanosheets:** The  $\text{V}_2\text{O}_5\text{-NH}_4^+$  nanosheets were prepared by one step calcination. 1 g  $\text{NH}_4\text{VO}_3$  (99%, Sigma-Aldrich) was calcined at 300 °C in the argon atmosphere with a heating speed of 5 °C/min and kept for 2 hours.

**Materials characterization:** The micromorphology and internal microstructure of the samples were investigated by scanning electron microscopy (SEM, TESCAN MIRA LMS, Czech Republic), transmission electron microscopy (TEM) and high-resolution transmission electron microscopy (HRTEM, JEM-2100). The phase composition of the samples was analyzed by X-ray diffraction (XRD, D8 Focus/Bruker). The 3D surface microstructure of the cycled Zn electrodes was probed with a laser scanning confocal microscope (LSCM, VK-X250). In situ optical images were captured during the Zn plating process using an optical microscope (Yuescope-YD650). Magnetic measurements were performed using Vibrating Sample Magnetometer (VSM, Lake Shore) and Magnetic Force Microscope (MFM, Bruker Nano).

**Electrochemical Measurements:** CR-2025 type coin cells were assembled under environmental conditions. The Battery Test System (LAND) was used to evaluate electrochemical performance of cells. A circular Zn foil with a diameter of 0.8 cm was used as the anode, The electrolyte was  $\text{ZnSO}_4$ , and a glass fiber separator (GF/A, Whatman) was used as the separator. All tests were conducted under atmospheric conditions. The  $\text{Zn} \parallel \text{Zn}$  symmetric cells

were used to compare the stability of the Zn plating/stripping. Coulombic efficiency (CE) measurements and plating/stripping curve were performed on Zn|Cu half cells. In a full cell test, the CFO-Zn or Bare Zn anode was reassembled with the NH<sub>4</sub><sup>+</sup>-V<sub>2</sub>O<sub>5</sub> cathode. the cathode plates were prepared by drop-casting a slurry containing NH<sub>4</sub><sup>+</sup>-V<sub>2</sub>O<sub>5</sub>, PVDF, and Super P with a mass ratio of 7:1:2 on Ti foils, followed by subsequent vacuum drying at 60 °C. The Tafel plots related to the corrosion behavior of the Zn electrodes was conducted in a three-electrode configuration with Zn foil, Pt plate, and Ag/AgCl as the working, counter, and reference electrodes, respectively. EIS (0.01-10<sup>5</sup> Hz at an amplitude of 5 mV) and CV (0.2-1.6 V) were investigated on an electrochemical workstation (CHI 660E).

### Calculation

The finite element calculation is based on COMSOL Multiphysics, simulating the movement process of ions in three-dimensional space under the action of electric field and electric field and magnetic field. The three-dimensional model has dimensions of 10×10×5 nm<sup>3</sup>, with a lower region of 4nm height designated as a mixed magnetic and electric field zone. The upper 1nm region is allocated for the electric field, with a 1nm region used for electric field acceleration. Boundary condition settings: the electric field above the three-dimensional region is set as positive and below is set as negative, with an electric field intensity of 188 V m<sup>-1</sup>. Particle properties are set as zinc ions with two positive charges, an electric power coupling interface is added, and the electric field intensity is derived from the electrostatic module. Zinc ion inlets are set in the positive electrode region with a random distribution selected, and an initial velocity of 0 m s<sup>-1</sup> is set. The mesh utilizes tetrahedral division with a total of 47,080 grids and a minimum mesh quality of 0.226. The electrostatic module adopts steady-state solving, while the particle tracking module employs transient solving. The steady-state solved electric field intensity is assigned to the particle tracking module to calculate the movement of charged particles in the electric field. The lateral magnetic potential is set to 4×10<sup>-6</sup> Wb m<sup>-1</sup> with a height of 4nm, oriented perpendicular to the wall surface outward. The magnetic potential can be converted into the magnetic induction intensity in each region using the curl formula to achieve a non-uniform distribution of the magnetic field. The curl formula is as follows:

$$\nabla \times B = \left( \frac{\partial R}{\partial y} - \frac{\partial Q}{\partial z} \right) i + \left( \frac{\partial P}{\partial z} - \frac{\partial R}{\partial x} \right) j + \left( \frac{\partial Q}{\partial x} - \frac{\partial P}{\partial y} \right) k$$

Where i, j, and k are the unit vectors along the coordinate axes, F represents the magnetic induction intensity B, P, Q, and R denote the components of magnetic induction B in three directions, and the values in parentheses are the components of magnetic potential in the three directions.

The equation for the motion of charged particles in an electromagnetic field is as follows:

$$F = qE + q(v \times B)$$

Where  $q$  represents the charge,  $E$  represents the electric field intensity,  $v$  represents the particle velocity, and  $B$  represents the magnetic induction intensity.

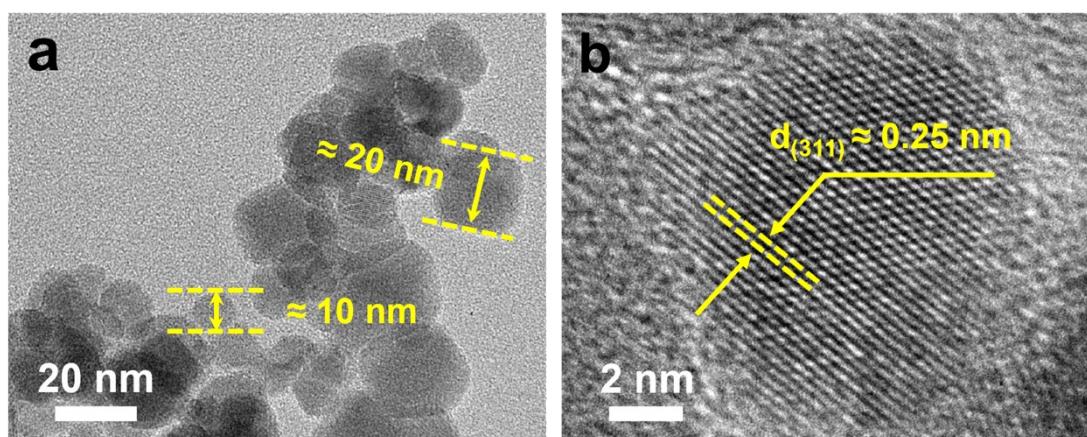


Fig. S1 (a) TEM and (b) HRTEM images of CFO.

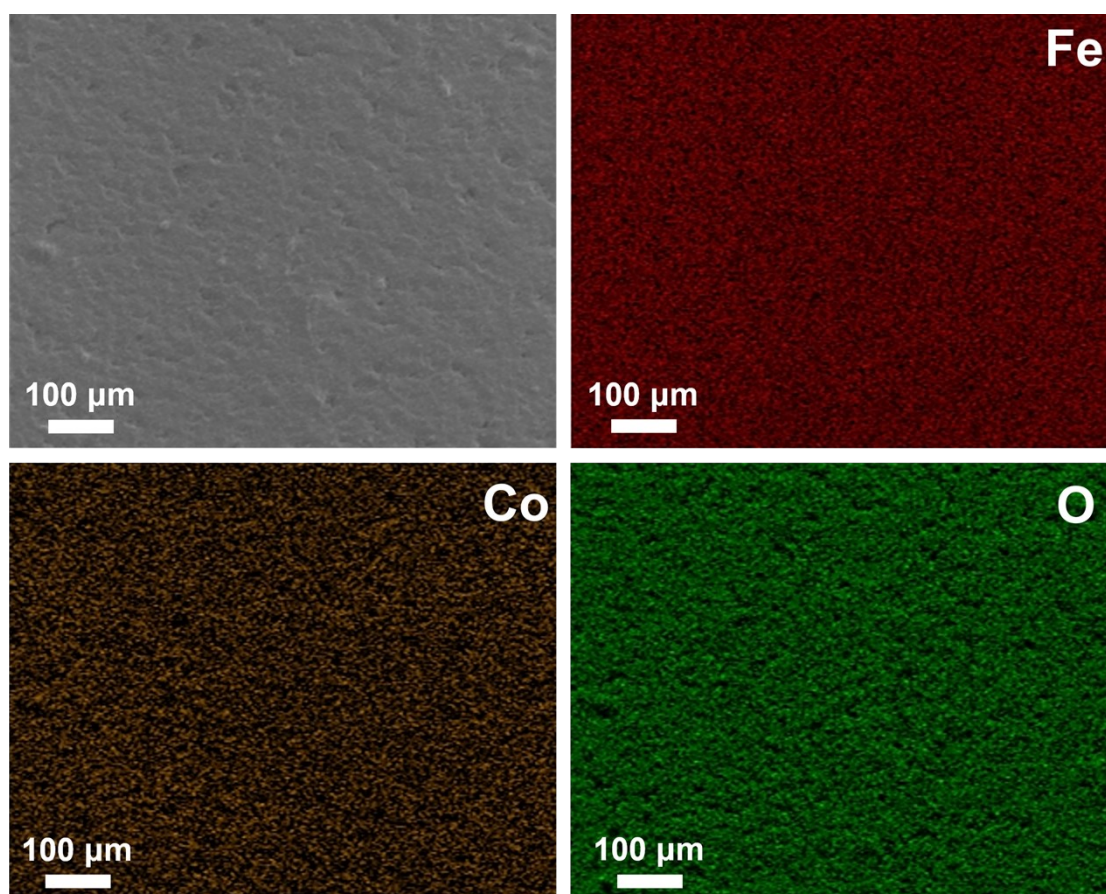
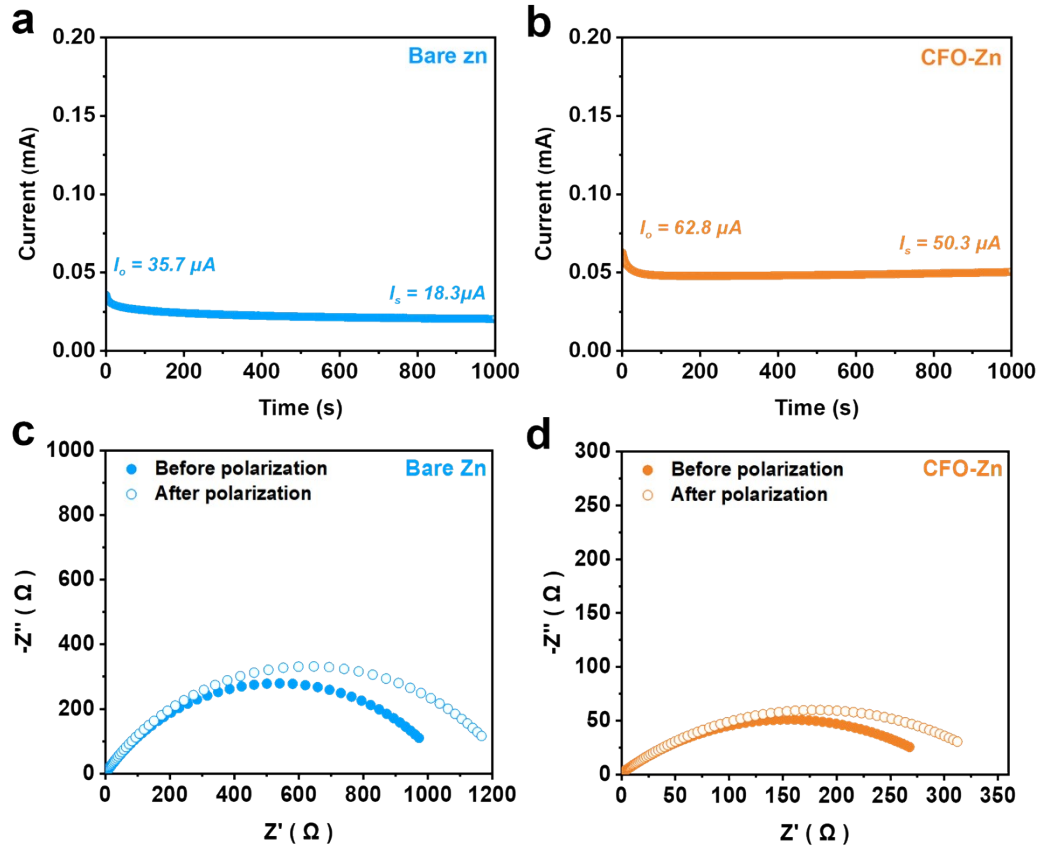


Fig. S2 SEM and corresponding EDS elemental mapping images of the CFO-Zn.



**Fig. S3** Direct-current polarization at a constant voltage of 25 mV for 1000 s: (a) Zn||Zn and (b) CFO-Zn||CFO-Zn symmetrical cells. EIS Nyquist plots of (c) Zn||Zn and (d) CFO-Zn||CFO-Zn symmetrical cells before and after polarization.

The transference number of  $Zn^{2+}$  ( $t_{Zn^{2+}}$ ) was evaluated in Zn||Zn symmetrical cells by alternating-current impedance and direct-current polarization techniques. The constant polarization voltage ( $\Delta V$ ) was set to 25 mV and  $t_{Zn^{2+}}$  was calculated according to the following equation:

$$t_{Zn^{2+}} = \frac{I_s(\Delta V - I_o R_o)}{I_o(\Delta V - I_s R_s)}$$

where  $I_o$  and  $I_s$  are the initial and steady-state currents,  $R_o$  and  $R_s$  are the initial and steady-state interfacial resistance.

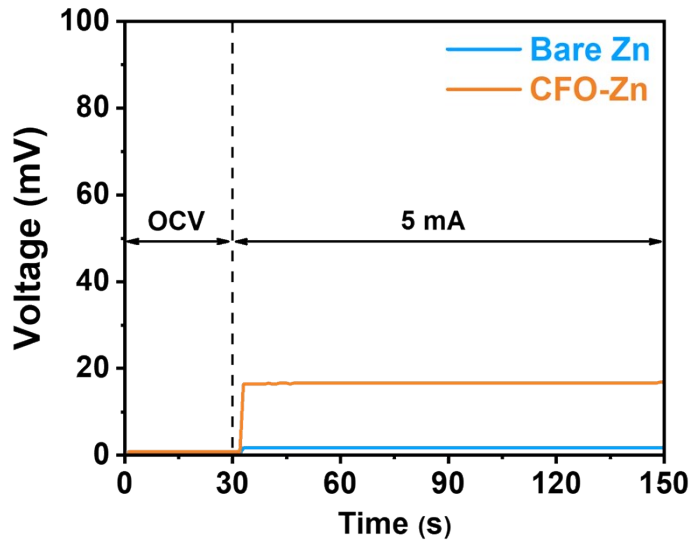


**Fig. S4** Voltage-time profiles of the bare Zn and CFO-Zn at the open circuit voltage (OCV) followed by a constant current of 5 mA. The electronic conductivity of the bare Zn or CFO-Zn was measured by sandwiching the bare Zn or CFO-Zn between two blocking electrodes (stainless steel sheets) with an applied current of 5 mA.

The electrical resistivity ( $\rho$ ) was calculated according to the following equation:

$$\rho = \frac{R \cdot S}{L} = \frac{U \cdot S}{I \cdot L}$$

Where  $L$  is the thickness of the samples,  $I$  is the applied current (5 mA),  $R$  is the resistance,  $S$  is the contact area ( $0.5 \text{ cm}^2$ ), and  $U$  is the average voltage. The calculated value of electric resistivity for the bare Zn ( $100 \text{ }\mu\text{m}$ ) is as follows:  $\rho = (2.0 \text{ mV} \times 0.5 \text{ cm}^2) / (5 \text{ mA} \times 100 \text{ }\mu\text{m}) = 17 \text{ }\Omega \text{ cm}^{-1}$  ( $\sigma_{\text{Zn}} = 5.882 \times 10^{-2} \text{ S cm}^{-1} = 58.82 \text{ mS cm}^{-1}$ ). Estimated from the voltage difference between the Zn and CFO APL, the electric resistivity of  $6 \text{ }\mu\text{m}$ -thick CFO APL film is as follows:  $\rho = [(17.0 - 2.0) \text{ mV} \times 0.5 \text{ cm}^2] / (5 \text{ mA} \times 6 \text{ }\mu\text{m}) = 2.533 \times 10^3 \text{ }\Omega \text{ cm}^{-1}$  ( $\sigma_{\text{CFO}} = 3.9 \times 10^{-4} \text{ S cm}^{-1} = 0.39 \text{ mS cm}^{-1}$ ).

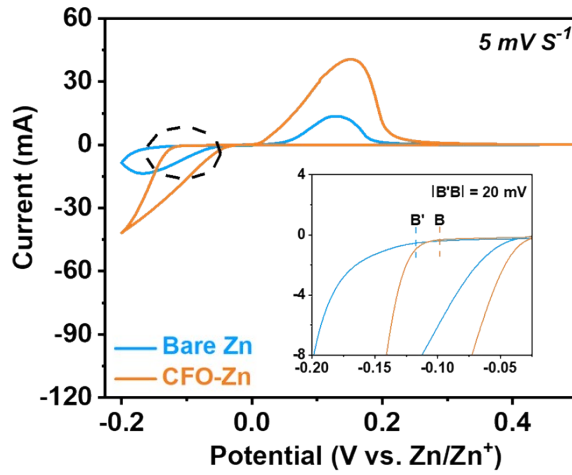


Fig. S5 CV curves of the bare Zn || Ti and CFO-Zn || Ti asymmetric cells.

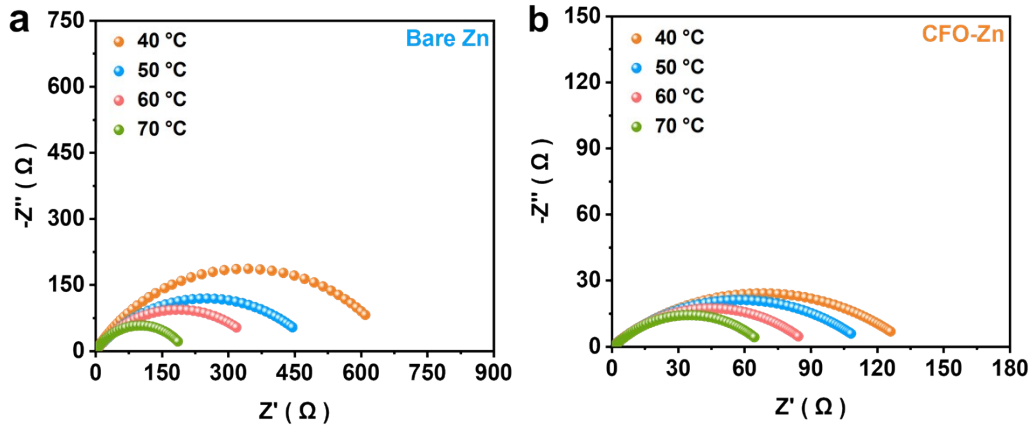


Fig. S6 EIS Nyquist plots of the (a) bare Zn and (b) CFO-Zn symmetric cells at various temperatures ranging from 40 to 70 °C.

The activation energy ( $E_a$ ) representing the desolvation barrier of  $Zn^{2+}$  was calculated by the Arrhenius equation using EIS data at various temperatures.

$$\frac{1}{R_{ct}} = A_0 \exp\left(-\frac{E_a}{RT}\right)$$

Where  $R_{ct}$ ,  $A_0$ ,  $R$ , and  $T$  denote the charge transfer resistance, frequency factor, ideal gas constant, and absolute temperature, respectively.

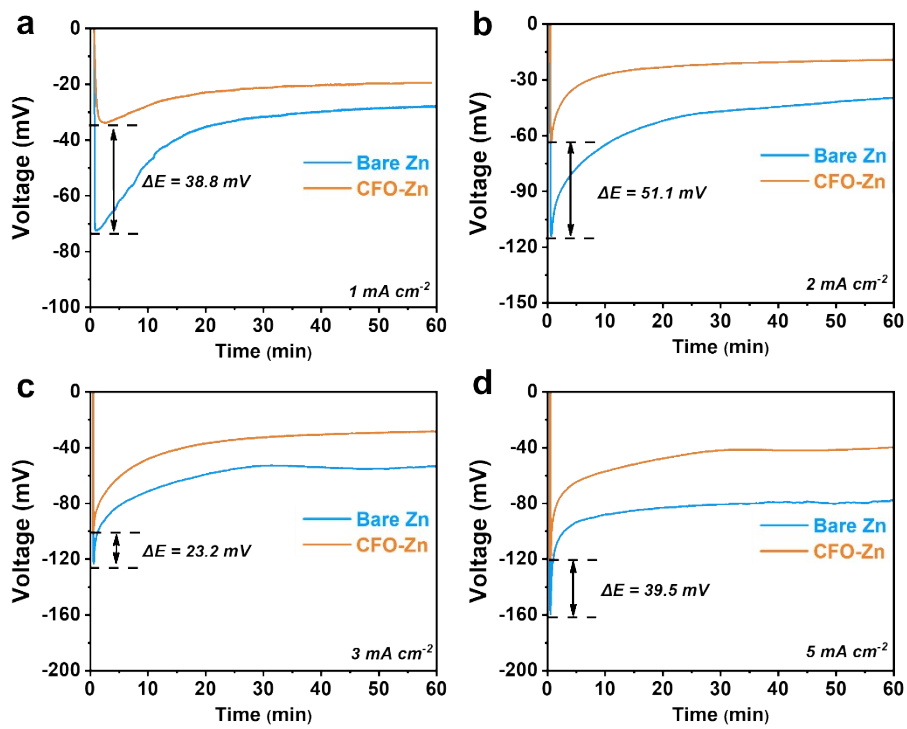


Fig. S7 Voltage-time profiles of the bare Zn || Cu and CFO-Zn || Cu half-cells obtained at (a)  $1 \text{ mA cm}^{-2}$ , (b)  $2 \text{ mA cm}^{-2}$ , (c)  $3 \text{ mA cm}^{-2}$ , and (d)  $5 \text{ mA cm}^{-2}$  during the initial Zn deposition process.

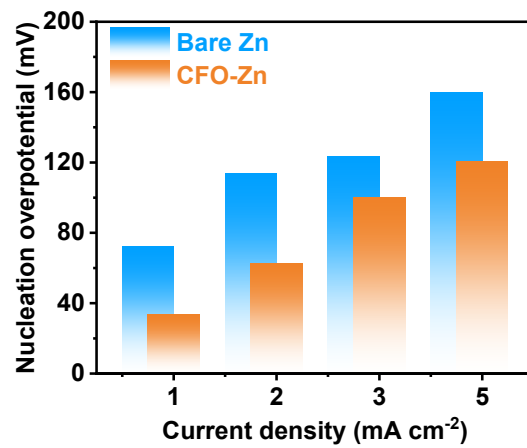
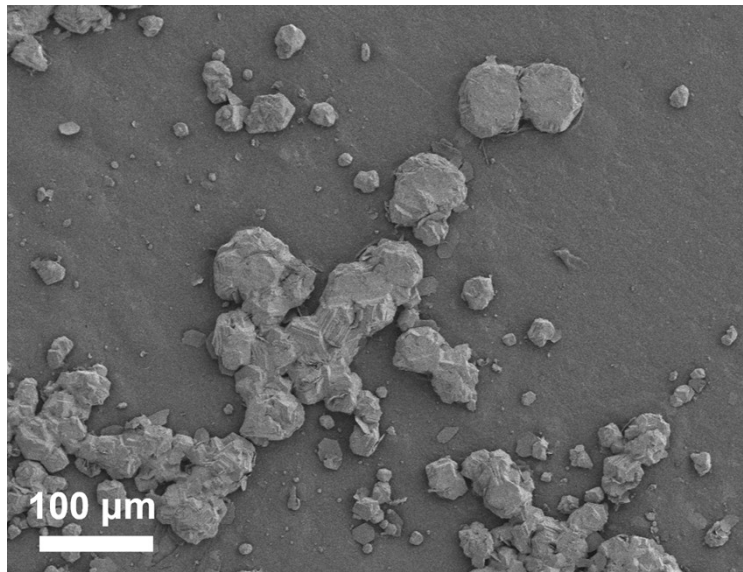
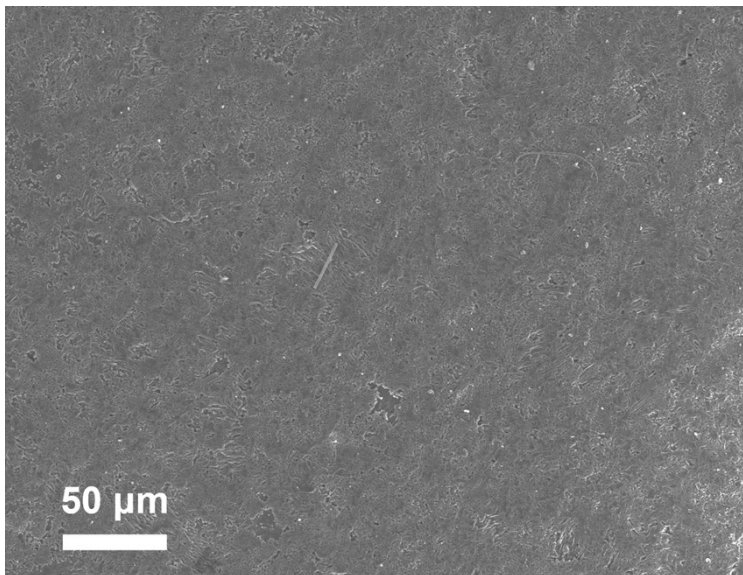


Fig. S8 Nucleation overpotentials of the bare Zn and CFO-Zn at various current densities.



**Fig. S9** SEM image of the bare Zn after 60 min plating at 5 mA cm<sup>-2</sup>.



**Fig. S10** SEM image of the CFO-Zn after 60 min plating at 5 mA cm<sup>-2</sup>.

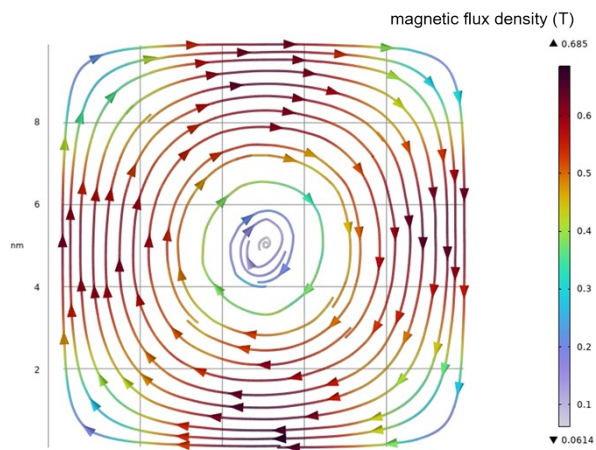


Fig. S11 The distribution of the non-uniform magnetic fields.

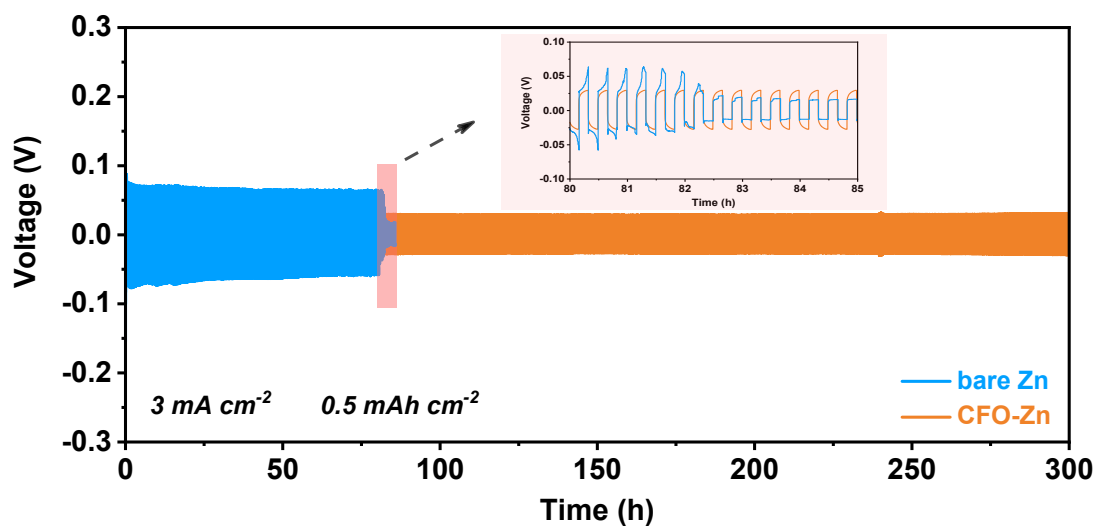


Fig. S12 Voltage-time profiles of the bare Zn and CFO-Zn symmetric cells at  $3 \text{ mA cm}^{-2}$  and  $0.5 \text{ mAh cm}^{-2}$ .

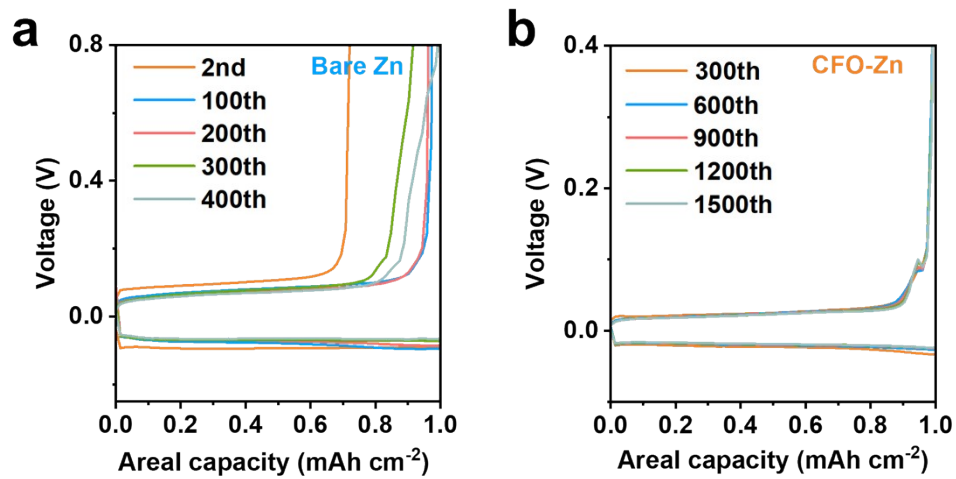


Fig. S13 Voltage-capacity curves of the (a) bare Zn || Cu and (b) CFO-Zn || Cu half-cells.

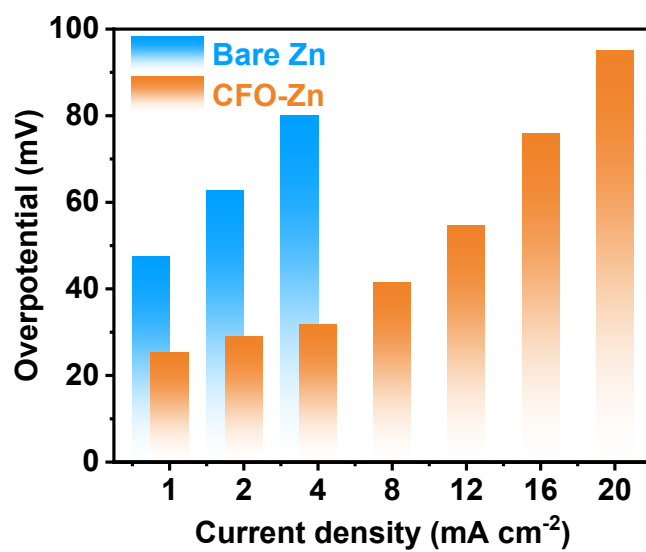


Fig. S14 Voltage hysteresis of the bare Zn and CFO-Zn symmetric cells under various current densities with a fixed capacity of 1 mAh cm<sup>-2</sup> obtained from Fig. 5b.

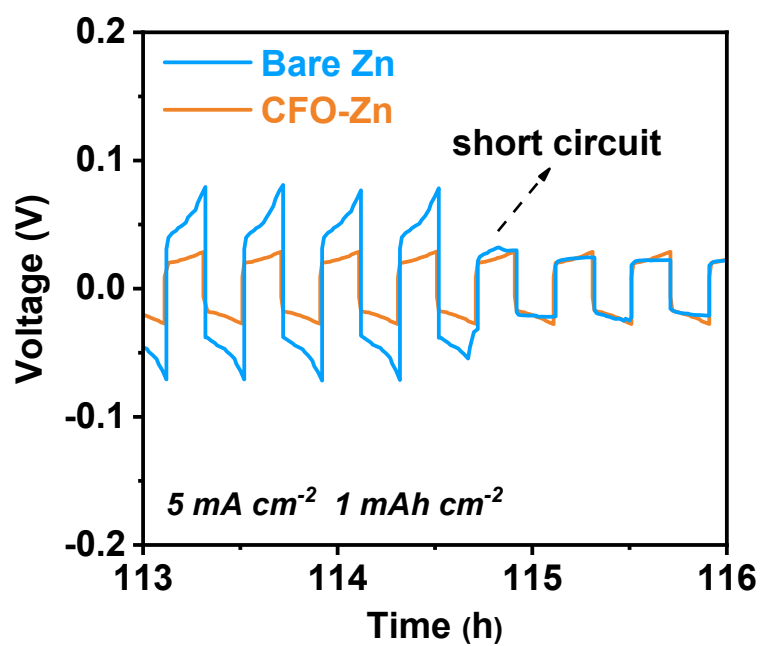


Fig. S15 Voltage-time profiles of the bare Zn and CFO-Zn symmetric cells at the representative cycles.

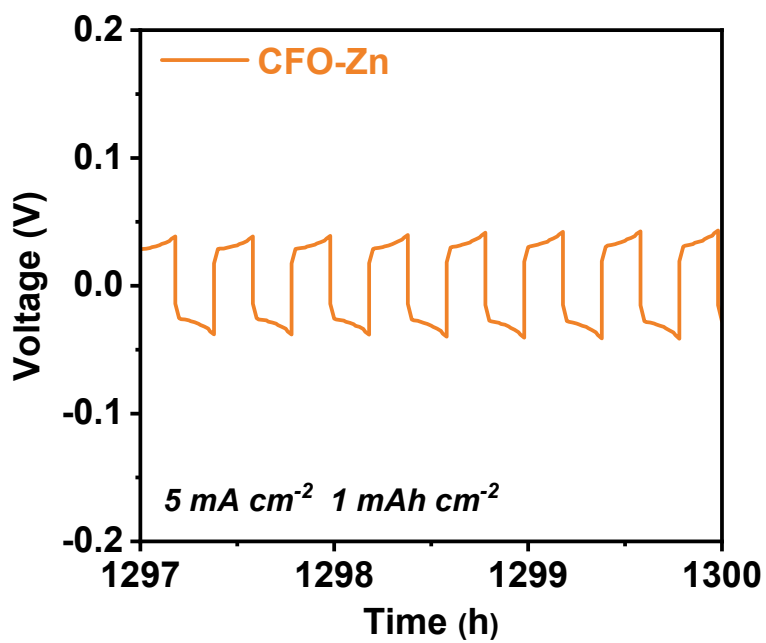


Fig. S16 Voltage-time profile of the CFO-Zn symmetric cell at the representative cycles.

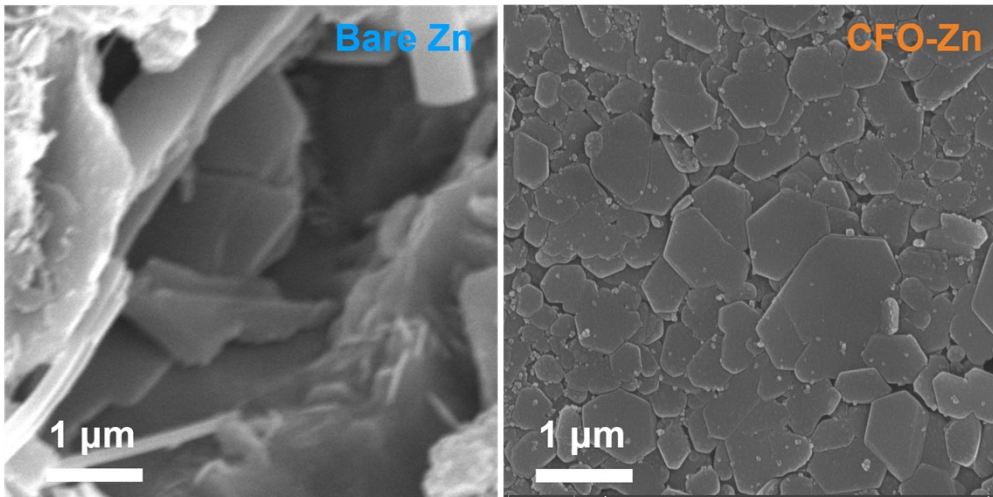


Fig. S17 SEM images of the bare Zn and CFO-Zn after cycling.

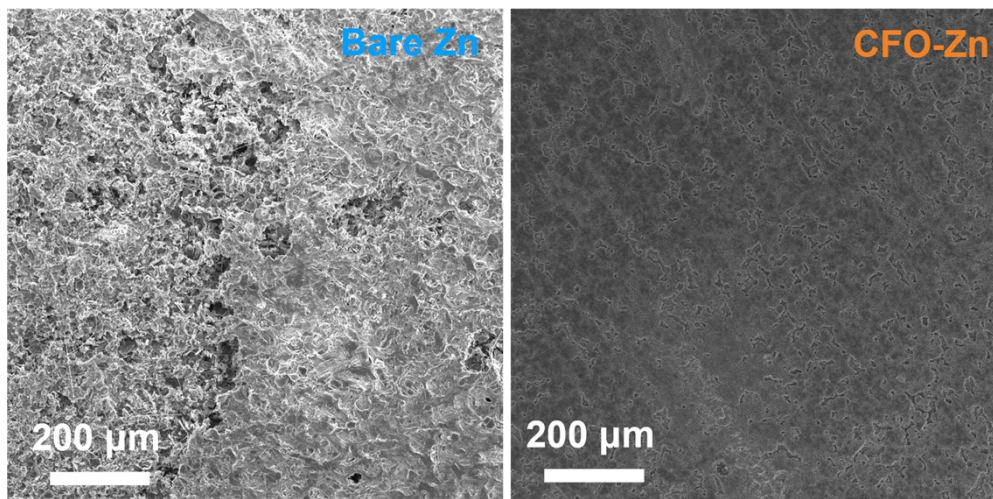


Fig. S18 SEM images of the bare Zn and CFO-Zn after cycling.

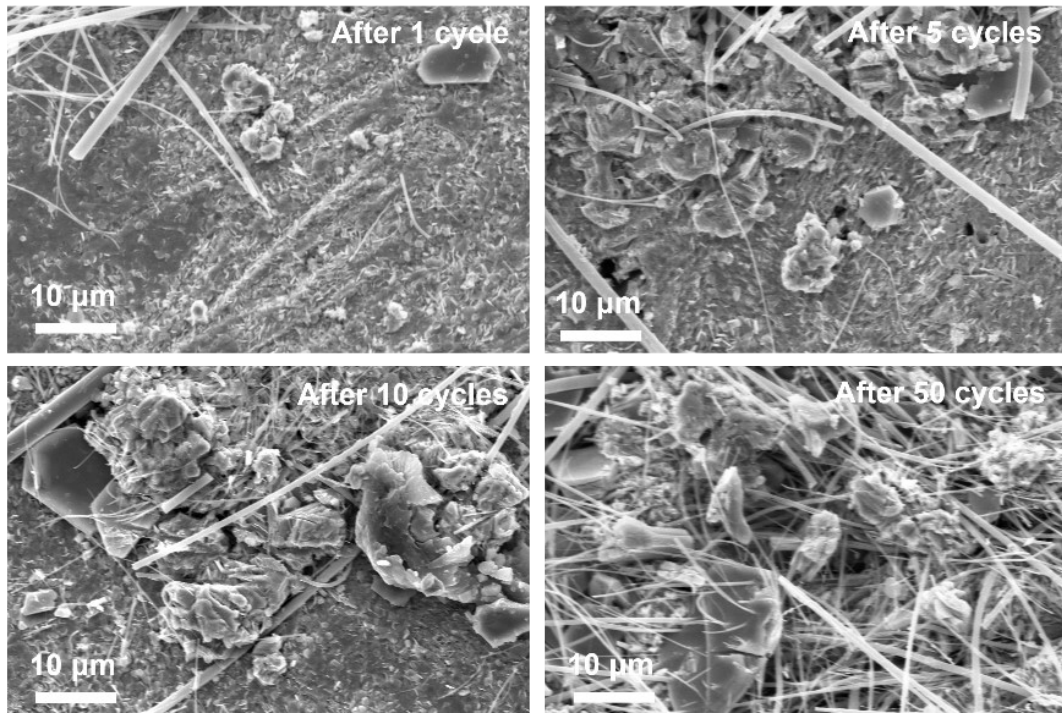


Fig. S19 SEM images of the bare Zn after different cycles.

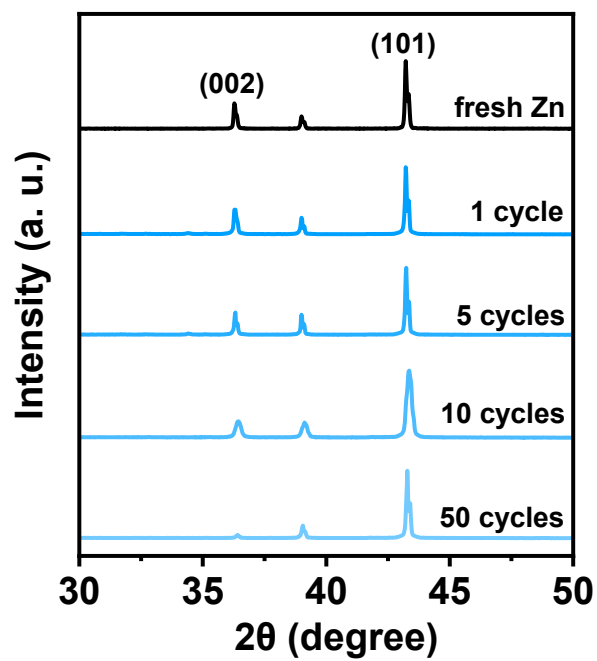


Fig. S20 XRD patterns of the bare Zn after different cycles.

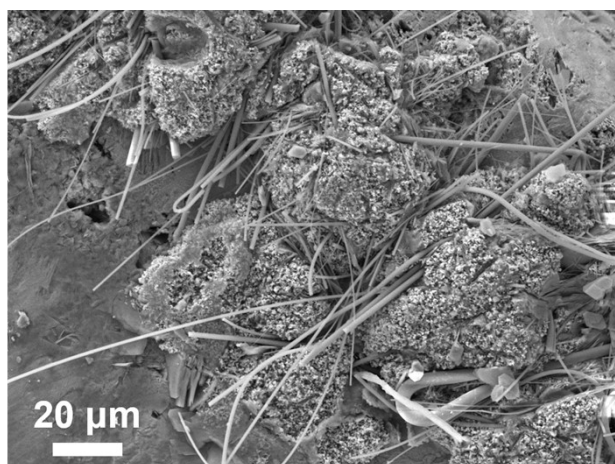


Fig. S21 SEM image of bare Zn after cycling at a high current density of  $20 \text{ mA cm}^{-2}$ .

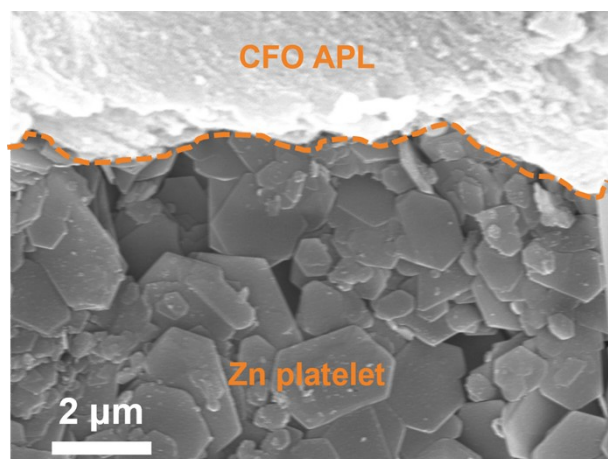


Fig. S22 SEM image of CFO-Zn after cycling at a high current density of  $20 \text{ mA cm}^{-2}$ .

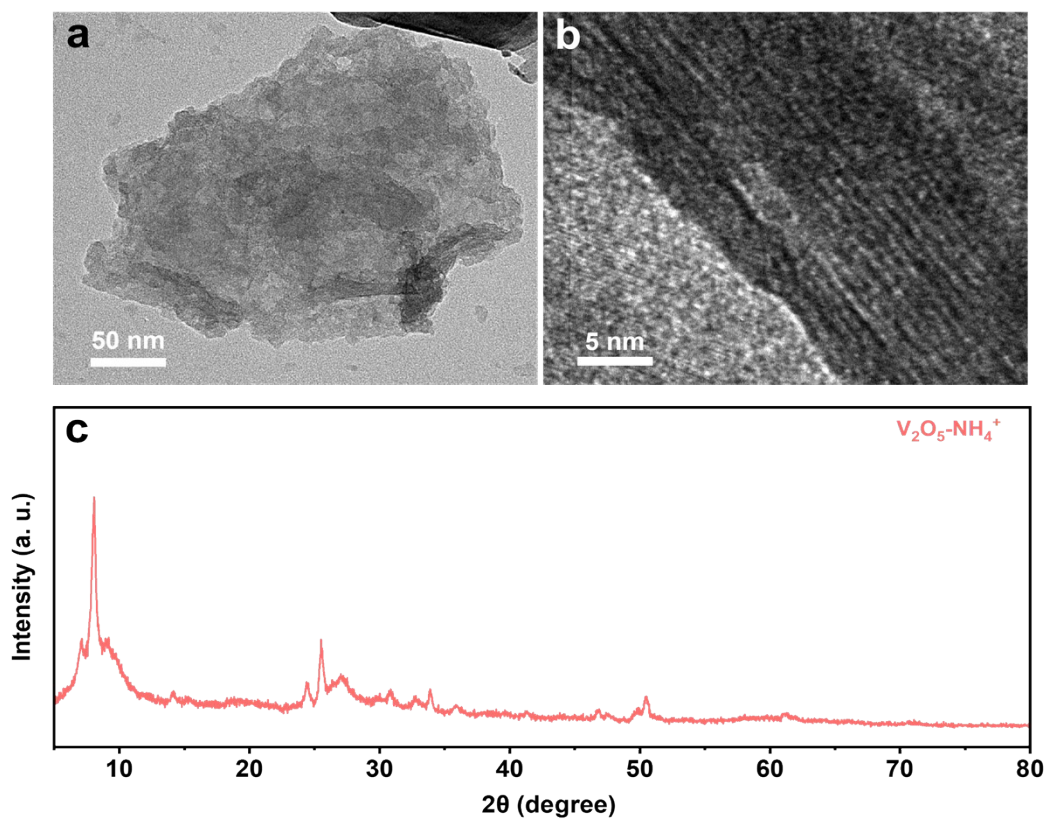


Fig. S23 (a) TEM image, (b) HRTEM image, and (c) XRD pattern of  $\text{V}_2\text{O}_5\text{-NH}_4^+$ .

Fig. S23 shows the TEM images and XRD pattern of the  $\text{NH}_4^+$ -intercalated  $\text{V}_2\text{O}_5$ , which align well with a previously reported study.<sup>1</sup>

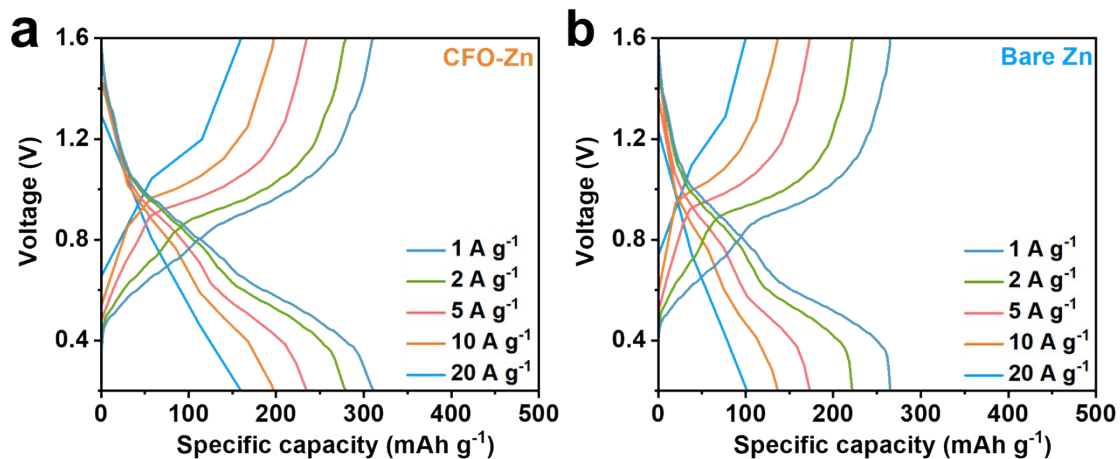


Fig. S24 Charging and discharging curves of the (a) CFO-Zn and (b) bare Zn based full cells at various current densities.

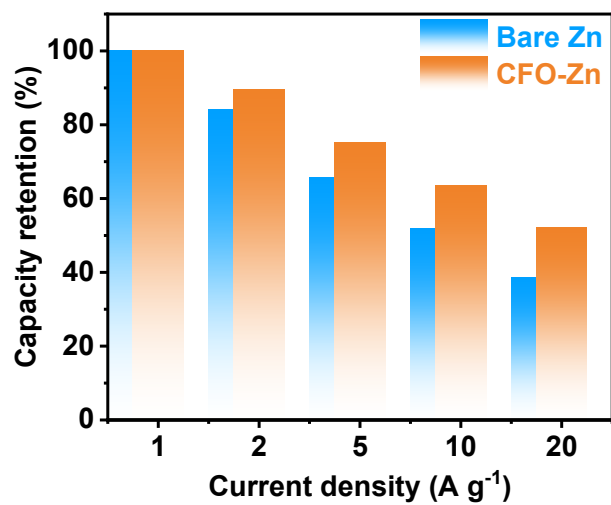
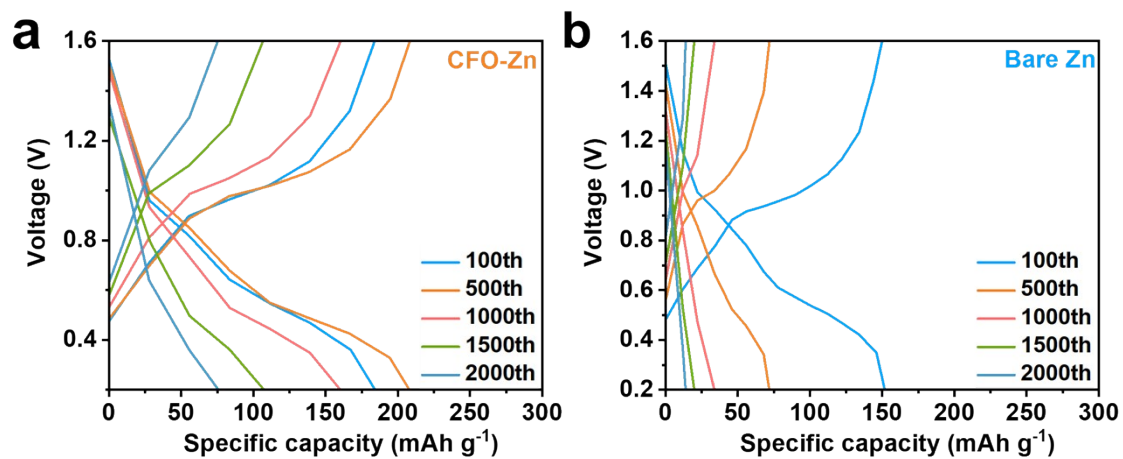
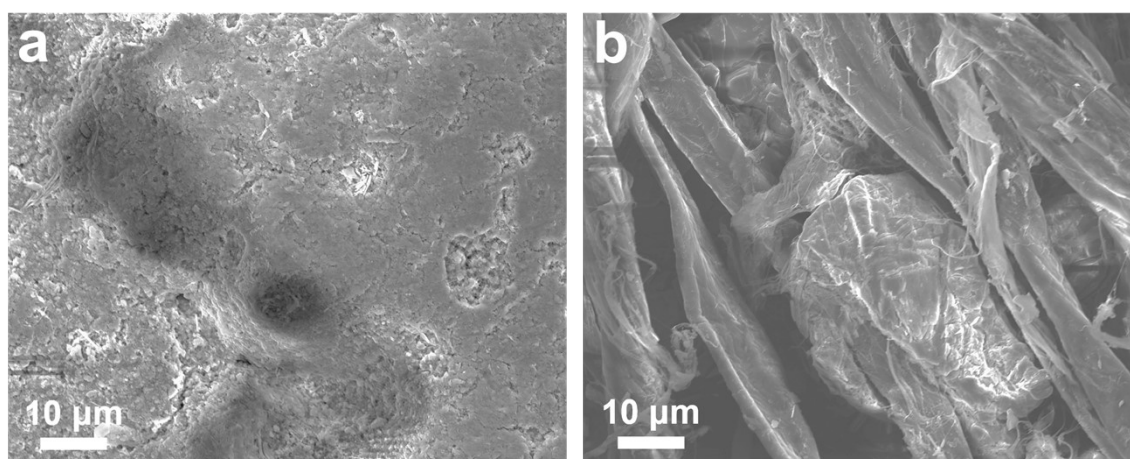


Fig. S25 Capacity retention of the bare Zn || V<sub>2</sub>O<sub>5</sub>-NH<sub>4</sub><sup>+</sup> and CFO-Zn || V<sub>2</sub>O<sub>5</sub>-NH<sub>4</sub><sup>+</sup> cells at different current densities.



**Fig. S26** Charging and discharging curves of the (a) CFO-Zn and (b) bare Zn based full cells at different cycles.



**Fig. S27.** SEM images of the (a) CFO-Zn and (b) bare Zn after cycling test.



**Fig. S28** Digital image of the CFO-Zn || V<sub>2</sub>O<sub>5</sub>-NH<sub>4</sub><sup>+</sup> cell glowing the LED lights.

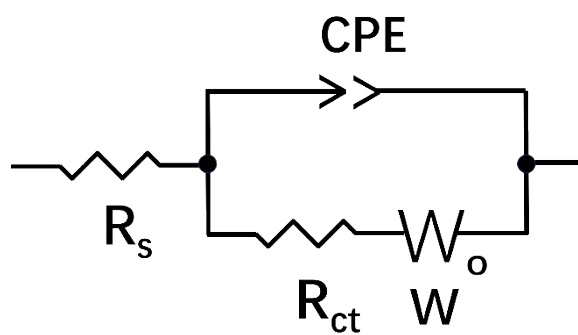


**Fig. S29** The fitting equivalent circuit of the CFO-Zn || V<sub>2</sub>O<sub>5</sub>-NH<sub>4</sub><sup>+</sup> and Zn || V<sub>2</sub>O<sub>5</sub>-NH<sub>4</sub><sup>+</sup> cells.

**Table S1.** The comparison of CFO-Zn with recently reported Zn anodes with surface modification.

Electrodes	Current density (mA cm <sup>-2</sup> )	Plating capacity (mAh cm <sup>-2</sup> )	Cycle number	Ref.
<b>CFO-Zn</b>	<b>5</b>	<b>1</b>	<b>1500</b>	<b>This work</b>
Zn@PAQ	4	1	1200	2
NGO@Zn	5	1	250	3
PDMS@TiO <sub>2-x</sub>	0.5	0.5	450	4
ZnSe@Zn	2	0.5	400	5
ZnS@Zn	2	1	200	6
Zn@CCF	1.13	0.57	120	7
Zp@Zn	1	1	350	8
C-ZSL@Zn	1	0.5	450	9
MMT-Zn	1	0.5	50	10
Zn@Bi/Bi <sub>2</sub> O <sub>3</sub>	4	1	1000	11
Zn@ZnO-3D	2	0.5	300	12
SEI-Zn	1	1	200	13
PANZ-Zn	0.5	0.5	200	14
CD-MWCNT@Zn	2	1	300	15

**Table S2.** The electrochemical impedance fitting parameters according to the equivalent circuit model shown in Fig. S29.

Samples	$R_{ct}$ (fresh)	$R_{ct}$ (after 50 cycles)	$R_{ct}$ (after 100 cycles)
Bare Zn	816.2	213.5	183.3
CFO-Zn	598.1	159.3	71.2

## References

1. Y. Wang, S. Wei, Z. H. Qi, S. Chen, K. Zhu, H. Ding, Y. Cao, Q. Zhou, C. Wang, P. Zhang, X. Guo, X. Yang, X. Wu and L. Song, *Proc. Natl. Acad. Sci. USA*, 2023, **120**, e2217208120.
2. Z. Zheng, D. Ren, Y. Li, F. Kang, X. Li, X. Peng and L. Dong, *Adv. Funct. Mater.*, 2024, **34**, 2312855.
3. J. Zhou, M. Xie, F. Wu, Y. Mei, Y. Hao, R. Huang, G. Wei, A. Liu, L. Li and R. Chen, *Adv. Mater.*, 2021, **33**, e2101649.
4. Z. Guo, L. Fan, C. Zhao, A. Chen, N. Liu, Y. Zhang and N. Zhang, *Adv. Mater.*, 2022, **34**, e2105133.
5. X. Yang, C. Li, Z. Sun, S. Yang, Z. Shi, R. Huang, B. Liu, S. Li, Y. Wu, M. Wang, Y. Su, S. Dou and J. Sun, *Adv. Mater.*, 2021, **33**, e2105951.
6. J. Hao, B. Li, X. Li, X. Zeng, S. Zhang, F. Yang, S. Liu, D. Li, C. Wu and Z. Guo, *Adv. Mater.*, 2020, **32**, e2003021.
7. C. Deng, X. Xie, J. Han, B. Lu, S. Liang and J. Zhou, *Adv. Funct. Mater.*, 2021, **31**, 2103227.
8. Z. Xing, Y. Sun, X. Xie, Y. Tang, G. Xu, J. Han, B. Lu, S. Liang, G. Chen and J. Zhou, *Angew. Chem. Int. Ed.*, 2023, **62**, e202215324.
9. J. H. Park, C. Choi, J. B. Park, S. Yu and D. W. Kim, *Adv. Energy Mater.*, 2023, **14**, 2302493.
10. H. Yan, S. Li, Y. Nan, S. Yang and B. Li, *Adv. Energy Mater.*, 2021, **11**, 2100186.
11. X. Tian, Q. Zhao, M. Zhou, X. Huang, Y. Sun, X. Duan, L. Zhang, H. Li, D. Su, B. Jia and T. Ma, *Adv. Mater.*, 2024, **36**, e2400237.
12. S. Jiao, J. Fu, M. Wu, T. Hua and H. Hu, *ACS Nano*, 2022, **16**, 1013-1024.
13. S. Di, X. Nie, G. Ma, W. Yuan, Y. Wang, Y. Liu, S. Shen and N. Zhang, *Energy Storage Mater.*, 2021, **43**, 375-382.
14. J. Yang, S. Wang, L. Du, S. Bi, J. Zhu, L. Liu and Z. Niu, *Adv. Funct. Mater.*, 2024, **34**, 2314426.
15. L. Kang, K. Yue, C. Ma, H. Yuan, J. Luo, Y. Wang, Y. Liu, J. Nai and X. Tao, *Nano Lett.*, 2024, **24**, 4150-4157.